ChemPubSoc Europe

DOI: 10.1002/celc.201901801

CHEMELECTROCHEM Articles

Special Collection

Single Molecule Conductance of Electroactive Helquats: Solvent Effect

Viliam Kolivoška,[a] Jakub Šebera,[a] Lukáš Severa,[b] Gábor Mészáros,[c] Romana Sokolová,[a] Jindřich Gasior,[a] Jana Kocábová,[a] Joseph M. Hamill,[d] Lubomír Pospíšil,*[a, b] and Magdaléna Hromadová*[a]

A series of helquat molecules with increasing number of rings n was studied by electrochemical and break junction methods to provide redox characteristics and single molecule conductance properties. Even though selected species do not contain anchoring groups the molecular junction conductance was observed experimentally and depends strongly on the solvent used. Single molecule conductance *G* is almost two orders of magnitude higher in water environment compared to mesitylene, whereas the distribution of *G* values is narrow in water and wide in mesitylene solvent. In the non-polar environment, *G* increases with increasing n, contrary to generally accepted notion of decreasing tunneling current with increasing molecular length. This behavior is, however, consistent with electrochemical properties, which showed that longer helquats are reduced more easily than the shorter ones. Furthermore, theoretical computations provided most probable molecular junction configurations of helquats in water solvent with excellent agreement between theoretical and experimental *G* values.

1. Introduction

Helicenes, known for a long time,[1] became more available and attractive after the development of new synthetic routes.[2] Azoniahelicenes are *N*-heteroaromatic dications derived from helicenes. They are also named helquats based on their structural similarity to well-known herbicide diquat (1,1′-ethylene-2,2′-bipyridyldiylium dibromide or IUPAC name 6,7-dihydro-dipyrido[1,2-*a*:2′,1′-*c*]pyrazinediium dibromide). The helquat structures used in this work (see Figure 1) contain five, six and seven rings that specify their names, in our case [5] helquat, [6]helquat and [7]helquat, respectively.

The synthesis of helquats is based on [2+2+2] cycloisomerization using Wilkinson's catalyst.[3] Helquats yield electrochemical properties very similar to diquat, which was demonstrated on [5]helquat and its four methylated derivatives previously.[4] For these molecules the electron transfer (ET) in aprotic solvents involves two separate one-electron reversible reduction steps. Racemic helquats can be separated into enantiomers labeled as [M] and [P], according to the rotation direction of their helices. Electron transfer of the chiral form leads to a profound reversible change of the electronic circular dichroism (ECD), even to a change of the sign of ECD signal.[5,6] Examples of recent applications of helicene-like compounds include enantioselective catalysis,[7] self-assembly,[8,9] surface science,[10] non-linear optics[11] and other fields. Of a particular interest are helicene-based switches,[12,13] which could find application as memory elements in molecular electronics. With respect to the last mentioned application this communication explores the relationship between electrochemical properties of helquat molecules and their single molecule conductance with particular focus on the effect of solvent environment.

Several recent works[14–17] have suggested that electrochemical characteristics of molecules can be correlated with their single molecule conductance properties. Thus molecules that were reduced or oxidized energetically more easily had higher single molecule conductance.

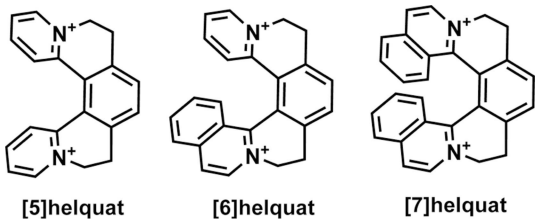

Figure 1. Chemical structures of helquat dications.

[a] Dr. V. Kolivoška, Dr. J. Šebera, Dr. R. Sokolová, Ing. J. Gasior, Dr. J. Kocábová, Dr. Dr. L. Pospíšil, Dr. M. Hromadová
Department of Electrochemistry at Nanoscale
J. Heyrovský Institute of Physical Chemistry of the Czech Academy of Sciences
Dolejškova 3, 18223 Prague, Czech Republic
E-mail: lubomir.pospisil@jh-inst.cas.cz
hromadom@jh-inst.cas.cz
[b] Dr. L. Severa, Dr. Dr. L. Pospíšil
Institute of Organic Chemistry and Biochemistry of the Czech Academy of Sciences
Flemingovo nám. 2, 16000 Prague, Czech Republic
[c] Dr. G. Mészáros
Research Centre for Natural Sciences, HAS
Magyar tudósok krt. 2, H-1117 Budapest, Hungary
[d] Dr. J. M. Hamill
School of Chemistry
University of Birmingham
Edgbaston B15 2TT, United Kingdom

Supporting information for this article is available on the WWW under https://doi.org/10.1002/celc.201901801

Special Collection *An invited contribution to a Special Collection dedicated to Giornate dell'Elettrochimica Italiana 2019 (GEI2019)*

The effect of solvent molecules on conductance values in metal-molecule-metal junctions was discussed only for bipyridine-based,[18] 1,4-benzenediamine-based,[19] oligoyne-based[20] and 1,4-benzenedicarboxaldehyde-based[21] molecules. In the latter case the precise tuning of the single molecule conductance was achieved by additional change of the electroactive salt concentration in the aqueous solution. Interestingly, three orders of magnitude higher conductance was observed for current-voltage characteristics of wet compared to dry Si-SAM-Hg junctions, where SAM stands for the alkene monolayer.[22] Finally, work of Fatemi et al.[19] stressed the importance of the interaction of solvent molecules with the gold substrate.

In this work we will discuss the effect of polar (water) and non-polar (mesitylene) solvent on the single molecule conductance of helquat molecules shown in Figure 1.

2. Results and Discussion

2.1. Electrochemistry

Heterogeneous electron transfer (ET) of helquat molecules involves two separate one-electron reductions leading to a cation radical and finally to a fully reduced neutral form. Both redox steps are reversible or quasi-reversible, depending on the experimental conditions. Typical cyclic voltammogram for [5]helquat and its derivatives was reported previously[3,4] together with a complete electrochemical, spectroelectrochemical and EPR characterization. Representative voltammogram for reduction of [6]helquat in acetonitrile is given in Figure 2 and for [7]helquat in Figure S-1 of the Supporting Information (SI).

Heterogeneous standard ET rate constants in acetonitrile were determined from the analysis of phase-sensitive AC polarograms measured in the frequency range from 16 Hz to 48 kHz (Figure S-2 in the SI) and from the electrochemical impedance spectroscopy (EIS) measurements from 5 Hz to 100 kHz. An appropriate vector analysis allows separation of the solution resistance, the double layer capacitance and finally the extraction of the faradaic phase angle ϕ. Figure 3 shows the dependence of cotϕ on the square root of angular frequency $\omega^{1/2}$, where the slope of this dependence is inversely proportional to the heterogeneous ET rate constant k^0.[23]

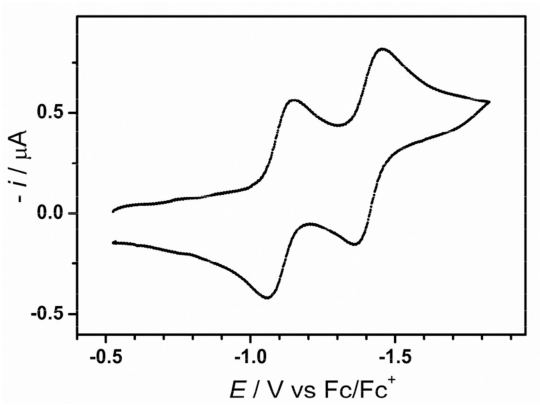

Figure 2. Cyclic voltammogram of 3.7×10^{-4} M [6]helquat in 0.1 M $TBAPF_6$ in acetonitrile using mercury drop electrode. The scan rate was 0.5 $V\cdot s^{-1}$.

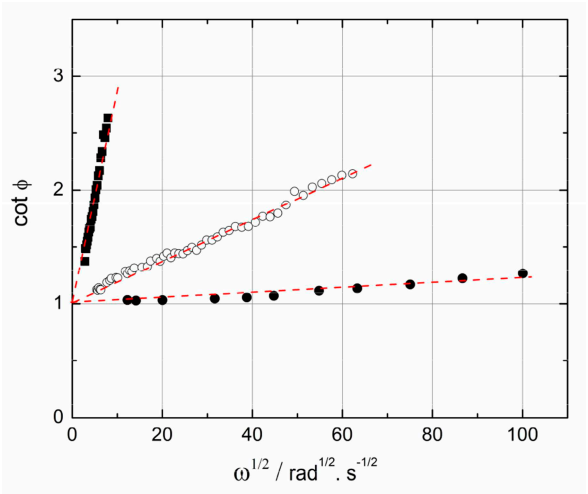

Figure 3. Faradaic phase angle as a function of the square root of angular frequency for [5]helquat (●), [6]helquat (○) and [7]helquat (■) for the first electron transfer step.

Standard redox potentials E^0 obtained from cyclic voltammograms and corresponding heterogeneous ET rate constants k^0 are given for both charge transfer steps in Table 1. The increasing number of rings n in helquat molecules shifts E^0 potentials towards less negative values, whereas k^0 values are decreasing with increasing n. Heterogeneous rate constant for the first redox step k^0_1 was found always smaller than k^0_2 for the second electron transfer. This trend was preserved for all three helquat molecules. Theoretical $E_1{}^0$ values obtained by quantum mechanical computations using DFT method (see Table 1) reproduce the shift of E^0 towards less negative potentials with increasing n very well. Experimental E^0 values correlate with the LUMO energies calculated for helquat molecules in the acetonitrile solvent (see Table 2) confirming LUMO as the

Table 1. Standard redox potentials and heterogeneous rate constants for the first and second electron transfer.

Molecule	E^0_1/V[a]	k^0_1 /cm·s^{-1}	E^0_2/V[a]	k^0_2/cm·s^{-1}	E^0_1/V[b]
[5]helquat	−1.248	1.22	−1.492	3.35	−1.368
[6]helquat	−1.103	0.15	−1.409	1.29	−1.291
[7]helquat	−1.053	0.037	−1.335	0.234	−1.248

[a] Experimental values against ferrocene/ferrocenium couple. [b] Calculated values against ferrocene/ferrocenium couple using DFT B3LYP method including the influence of acetonitrile solvent.

Table 2. Summary of molecular orbital energies in acetonitrile solvent.

Molecule[a]	HOMO/eV[b]	LUMO/eV[b]	LUMO-HOMO/eV[b]
[5]helquat	−7.59	−3.46	4.13
[6]helquat	−7.27	−3.53	3.74
[7]helquat	−7.26	−3.57	3.69

[a] Without triflate counterions. [b] DFT B3LYP method, PCM model for description of acetonitrile solvent.

electron accepting orbital. Additionally, the computed HOMO-LUMO gap decreases with increasing number of rings in the series of helquat molecules.

Redox processes in the aqueous medium are characterized by a single two-electron reduction accompanied by a strong adsorption of both oxidized and reduced forms (see Figure 4). Dications adsorb in the range of potentials −0.1 to −0.9V (the onset of reduction). Neutral fully reduced helquats are sparingly soluble in water and strongly suppress the value of the double layer capacitance for potentials more negative than −1.2V. The evaluation of kinetic data of adsorbing systems requires more elaborate separation of charging and kinetic parameters.[24] The adsorption of fully reduced forms of helquats in water makes the estimation of kinetic parameters practically impossible.[25] Strong adsorption in water contrasts very weak adsorption of these molecules in acetonitrile (see Figure S-2 of the SI).

2.2. Single Molecule Conductance

Helquats used in this work unlike other molecules investigated for single molecule conductance do not contain anchoring groups (–SH, $–NH_2$, pyridine, etc.). In spite of this fact dicationic helquats can form single molecule junctions and their adsorption properties are sufficient to obtain reliable conductance data for individual molecules.

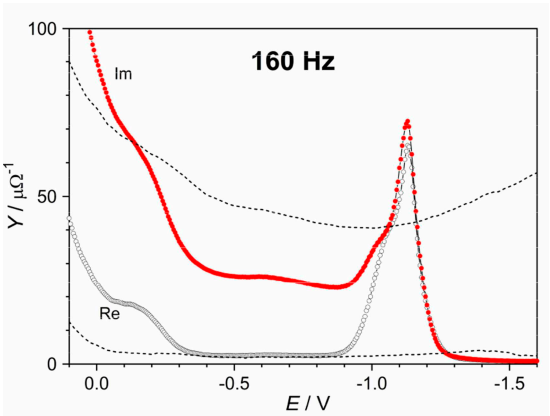

Figure 4. Phase sensitive AC polarogram of 5×10^{-4} M [5]helquat in the aqueous 0.1 M KF against Ag|AgCl|1 M LiCl reference electrode. Sine-wave frequency was 160 Hz. The real (Re) and imaginary (Im) admittance components are shown as black (○) and red (●) curves, respectively. Real and imaginary admittance components for the supporting electrolyte only are shown as dotted lines.

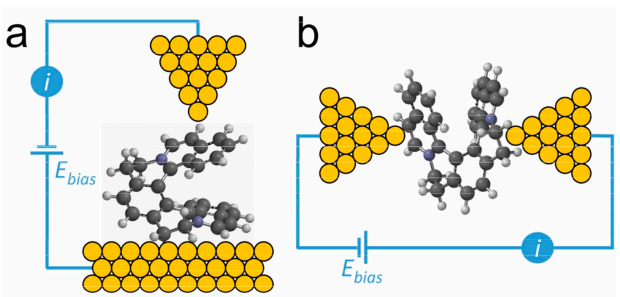

Figure 5. Schematic representation of (a) STM BJ and (b) MCBJ technique.

Single molecule conductance was obtained by two complementary techniques that enabled formation and breaking of thousands of gold-molecule-gold junctions. Current was measured at constant potential difference E_{bias} between two gold electrodes (see schematic representation in Figure 5) and converted to the conductance using Ohm's law. In the STM break junction (STM BJ) technique the STM tip makes initial contact to the gold substrate and current is measured as a function of the increasing distance between the gold tip and substrate electrodes. In the mechanically-controlled break junction (MCBJ) method a gold wire is broken as a consequence of the force inserted on the wire support and additional separation of thus created electrodes is achieved by a piezo element. The current-distance curves are obtained by this method too, but the electrode separation is not a simple function of the movement of the piezo element. More detailed explanation of both techniques is given elsewhere.[26,27]

Experimental data are presented on the logarithmic scale in the form of $\log(G/G_0)$ retraction curves (Figure 6a and 6d), where G is the conductance equal to i/E_{bias} and $G_0 = 77.5$ μS is the conductance quantum, which represents the atomic contact conductance for gold metal. Conductance-distance curves thus contain plateau at $\log(G/G_0)$ equal to 0 indicating the gold-gold atomic contact. In the absence of molecules at $\triangle z > 0$ nm only a tunneling current is observed, which corresponds to linearly decaying signal on the logarithmic scale. If the molecule bridges the electrodes an additional plateau is observed and the distance at which the contact breaks (sudden conductance decrease) can be used to infer the junction geometry and length of the molecule for fully extended junction geometries. Typical measurement involves collecting several thousands of conductance-distance traces (Figure 6a and 6d) evaluated statistically into a 2D conductance-distance histogram (Figure 6b and 6e) or a simpler 1D conductance histogram (Figure 6c and 6f), in which a peak indicates the most probable single molecule conductance value and its width the distribution of different molecular junction (MJ) configurations. The STM BJ method allows measurements in both aqueous (with insulated tips) and non-aqueous environment. Similar current transients are measured by the MCBJ technique; however, the assignment of the MJ length is based on several assumptions and is not reliable. Even though the MCBJ technique has lower noise level than the STM BJ method, the experiments can be performed only in the nonpolar solvents. Thus both methods were used for single molecule conductance measurement in mesitylene solvent and STM BJ method additionally in the aqueous environment. These two solvents represent two extremes in the polarity enabling studies of the effect of the environment on the charge transport in molecular junctions (MJs) without directional covalent anchoring to the electrodes.

Corresponding 1D histograms for helquats in water and mesitylene show a peak-like feature which represents the most probable single molecule conductance (see Figure 6a and 6d for [6]helquat). Table 3 summarizes the experimental $\log(G^{exp}/G_0)$ values obtained by both STM BJ and MCBJ methods.

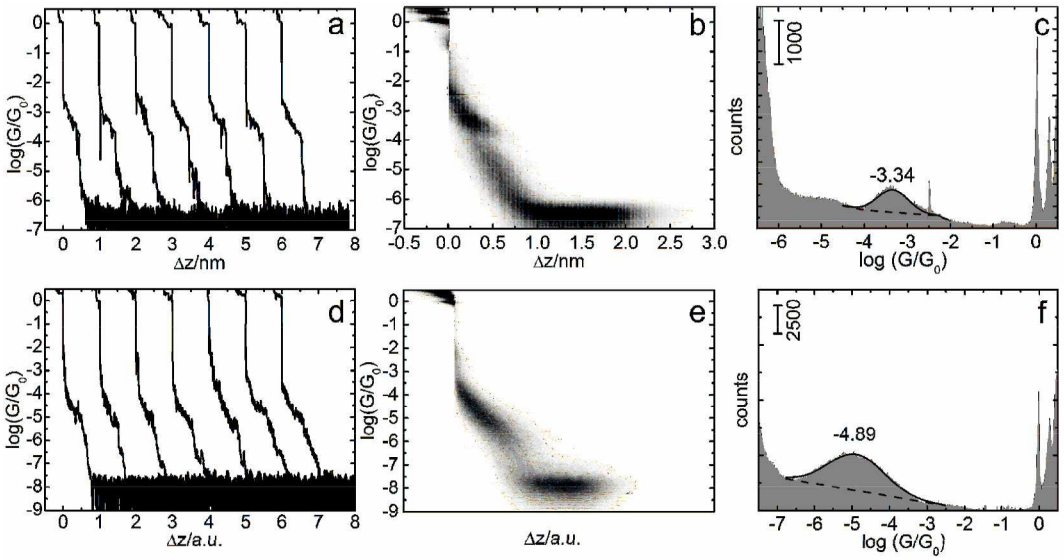

Figure 6. Single molecule conductance data for [6]helquat molecule showing representative individual conductance-distance transients (a,d), 2D conductance-distance histogram (b,e) and 1D conductance histogram (c,f). The upper row was obtained by STM BJ method in water (a,b,c) and bottom row by the MCBJ method in mesitylene (d,e,f).

Table 3. Summary of experimental values of single molecule conductance and molecular junction length.

Molecule	$\log(G^{exp}/G_0)$[a]	$\log(G^{exp}/G_0)$[b]	$\log(G^{exp}/G_0)$[c]	z^{exp}/nm[c]
[5]helquat	-5.1 ± 1.4	-5.1 ± 0.9	-3.3 ± 0.4	0.8 ± 0.2
[6]helquat	-4.9 ± 0.9	-4.9 ± 0.9	-3.3 ± 0.4	0.8 ± 0.1
[7]helquat	-4.6 ± 1.2	-4.7 ± 1.1	-3.3 ± 0.4	0.9 ± 0.2

[a] STM BJ method, mesitylene. [b] MCBJ method, mesitylene. [c] STM BJ method, water solvent.

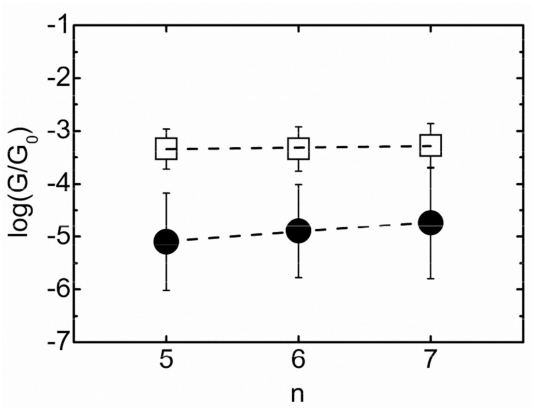

Figure 7. Single molecule conductance values for three helquat molecules of different length (n represents number of rings, see Figure 1) in water (□) and in mesitylene (●).

Reported errors represent half of the full width at half maximum of the conductance peak. The single molecule conductance values obtained in mesitylene solvent are independent of the experimental method used and show an increase in conductance from [5]helquat to [7]helquat. A considerable width of the observed features suggests that MJs formed in mesitylene undergo substantial rearrangement in the course of their evolution leading eventually to a rapid loss of electronic communication between the molecule and the electrodes (see Figures S-4 and S-5). On the other hand, aqueous environment supports highly conductive single molecule junctions with a narrow distribution of conductance values (see Figure S-3). This difference is manifested also in 1D conductance histograms of Figure 6 for [6]helquat as well as in Figure 7, which summarizes $\log(G^{exp}/G_0)$ values for all three helquats including the error bars. High conductance values and narrow peak width indicate that single molecule junctions formed in the aqueous environment are stable and possess well defined geometries.

In the aqueous environment the characteristic plateau length Δz for each helquat system was evaluated following a previously described procedure.[27] The most probable MJ length was obtained as $z^{exp}=\Delta z+z_{corr}$, where $z_{corr}=0.4$ nm represents the correction for the snap-back distance. The characteristic plateau length Δz histograms are shown in Figure S-6 of the SI.

Experimental data in Table 3 indicate that for all three helquats the MJ conductance is higher in the aqueous solvent than in mesitylene. In water both conductance values as well as the MJ lengths are identical for all three molecules indicating a significant contribution of the solvent in the tunneling process. At this point we should remind the reader that in the absence of molecules and in the presence of solvent the peak feature around $\log(G/G_0)\sim-3.3$ is absent in the 1D conductance and no plateau is observed in 2D conductance-distance histograms, so the observed features are uniquely associated with helquat molecules in the presence of the solvent environment (for histograms in the absence of molecules see Figure S-7 of the SI).

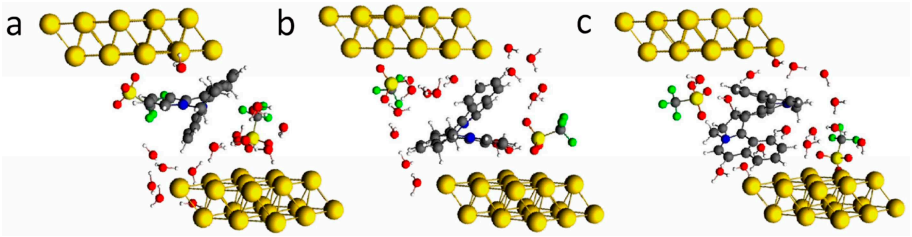

Figure 8. Representative (geometry optimized) molecular junction configurations for [5]helquat (a), [6]helquat (b) and [7]helquat (c) including 2 $CF_3SO_3^-$ counterions and 15 water molecules.

In the presence of mesitylene solvent the single molecule conductance increases from [5]helquat to [7]helquat (see Figure 7). Even though we were not able to use the same procedure as in the case of water solvent for a rigorous determination of the experimental MJ length z^{exp}, it can be inferred from data in Figure S-4 that the MJ length is either not very different from that observed in water environment or z^{exp} slightly increases with increasing n parameter. The observation of increasing $\log(G^{exp}/G_0)$ values with increasing number of rings n in helquat molecules is very interesting and goes against the generally assumed notion that molecular conductance should decrease with increasing molecular length. On the other hand we have observed that G^{exp} values correlate with E_1^0 values reported in Table 1. Thus, helquat molecule, which accepts electron more easily, i.e., has less negative standard redox potential, displays higher single molecule conductance.

Single molecule junctions of helquat dications were further analyzed theoretically by the approach based on the combination of density functional theory (DFT) and non-equilibrium Green's function (NEGF) formalism. Calculations considered a single helquat dication and two triflate anions to compensate the electric charge. Investigated species were positioned between two clusters, each composed of 18 gold atoms meant to represent electrodes mimicking the break junction arrangement (either STM BJ or MCBJ). The effect of solvent on the charge transport in the single molecule junctions was treated explicitly by adding 15 molecules of water to the molecular junction. The electrode separation L_{MJ} (measured as perpendicular distance between two planes involving centers of gold atoms facing the helquat molecule on each side of the junction) was fixed so that theoretical MJ length z^{th} becomes identical to the experimentally obtained MJ length extracted from the STM BJ based plateau length analysis (see z^{exp} values in Table 3 and z^{th} values in Table 4).

Theoretical analysis of the geometrical arrangement within MJ configurations typically relies on a variation of the distance between apex gold atoms of two electrodes that are chemically attached to anchoring groups of the molecule. Due to the absence of anchoring groups in investigated compounds and independence of the experimentally observed MJ length on the number of rings in the helquat molecules (z^{exp} in Table 3), we decided to consider the angle between the plane of the central benzene ring of the helquat molecule and the electrode surface θ as an independent variable to describe the geometrical arrangement of MJ configurations (see Figure S-7 of the SI). For representative junction configurations of helquat molecules this angle falls into the range between 22° and 37° indicating that the central benzene ring of all three helquats is slightly inclined with respect to the electrode surface. Such geometrical arrangement allows the inclusion of several water molecules between the electrodes. As confirmed experimentally, the presence of water leads to a dramatic enhancement of the charge transport and of the MJ stability (Figure 7) compared to the non-polar mesitylene environment. For each compound, several MJ configurations involving varied orientation of the helquat dication with respect to such fixed electrodes were constructed and their geometry was gradient optimized on the potential energy surface (see Table S-1 of the SI). The junction configuration with the lowest electronic energy was selected as the representative one and considered further (see Figure 8).

Transmission functions for helquats in the representative MJ configurations containing 15 water molecules are given in Figure 9. The theoretical value of the single molecule conductance G^{th} was derived from the transmission function value at the Fermi energy of gold in vacuum ($\varepsilon_F = -5.1 \pm 0.1$ eV) employing zero-bias approximation. For theoretically predicted single molecule conductance values in water G^{th} see Table 4 which summarizes also characteristic junction parameters z^{th} and θ. An excellent agreement was found between experimentally obtained G^{exp} and G^{th} in the case of water if the Fermi energy of gold in vacuum was used. The choice of ε_F for the electrodes in contact with different solvent molecules is not straightforward. We used the experimentally obtained value of ε_F in vacuum, even though multiple layers of water on Au(111) surface may decrease the work function by 0.6 eV .[28] Our choice is based on the fact that MJ configurations in Figure 8 do not contain even one solvation shell for the electrode

Table 4. Summary of theoretical single molecule conductance values and junction parameters.

Molecule	$\log(G^{th}/G_0)$[a]	$\log(G^{th}/G_0)$[b]	z^{th}/nm[c]	θ/°[c]
[5]helquat	-3.8 ± 0.1	-3.4 ± 0.1	0.76	36.7
[6]helquat	-3.2 ± 0.1	-3.4 ± 0.1	0.79	22.5
[7]helquat	-3.3 ± 0.1	-3.3 ± 0.1	0.85	24.0

[a] Vacuum. [b] 15 water molecules. [c] $z^{th} = L_{MJ}$-0.25 nm, L_{MJ} representing distance between two gold planes in molecular junction, θ is the angle defining position of helquat with respect to gold electrodes, see Figure S-8 of the SI.

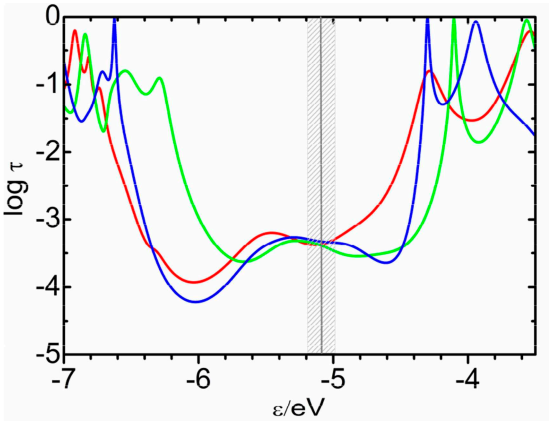

Figure 9. Transmission functions calculated for representative MJ configurations of [5]helquat (red line), [6]helquat (green line) and [7]helquat (blue line) in water solvent. Corresponding junction configurations are shown in Figure 8.

pointing to the role of helquat solvation in the charge transport process. Furthermore, electrochemical studies confirmed the tendency of helquats to adsorb at the charged electrode|aqueous electrolyte interface (see Figure 4). Our approach is consistent as well with that of Milan et al.,[29] who compared the calculated conductance values with experimental ones at different ε_F until the closest agreement was found. The closest agreement of our G^{th} with experiment is indeed for ε_F values close to -5.1 ± 0.1 eV (shaded area in Figure 9). In order to assess the effect of water molecules directly, the conductance was reevaluated for the same MJ configurations shown in Figure 8 in the absence of water molecules. This result is shown in the first column of Table 4 as G^{th} in vacuum. Such calculations correctly predict the trend of increasing conductance from [5]helquat to [7]helquat observed in mesitylene solvent. Both computations support two experimental observations. Primarily, the presence of water molecules allows for the existence of "representative" MJ configurations that provide conductance values identical with the experiment. Secondly, by omitting water molecules the G^{th} is no longer constant, but mimics the charge transport in mesitylene solvent, even though thus calculated G^{th} values are much higher compared to the experimental ones. We did not attempt further theoretical analysis of single molecule conductance in mesitylene, since we lack reliable information on the experimental MJ length and the peak shape clearly indicates wider distribution of MJ configurations, which must be taken into account. However, reported calculations correctly predict the trend of increasing conductance from [5]helquat to [7]helquat and point further to a decisive role of helquat molecules in their charge transport characteristics in mesitylene solvent.

There are only two reports on the single molecule conductance properties of uncharged diazahelicenes, where *N*-heteroatoms served as the anchoring groups.[30,31] In the first work the theoretical description of mechanical tuning of the single molecule conductance was emphasized, whereas in the second one the single molecule conductance of oxa[9]helicene terminated by pyridine units was reported to be 8.8×10^{-4} G/G_0 ($\log(G/G_0) = -3.06$), which is in reasonable agreement with our measurements assuming that this molecule has n equal to 9 and contains anchoring groups.

Despite the fact that MJs containing helquat dications lack covalent bonding with gold electrodes, such molecules are clearly capable of forming highly conductive charge transport channels in water solvent and less efficiently conductive ones in non-polar mesitylene. The outstandingly narrow distribution found for the conductance peak in the aqueous environment suggests that preferred MJ configurations exist in water and the transport of electric charge is not attenuated during the junction evolution as much as in mesitylene solvent. This observation is consistent with our observations that adsorption of helquat molecules on electrified interfaces (electrode) is enhanced in the presence of aqueous environment compared to other polar organic solvents (see Figure 4 and Figure S-2). This work clearly demonstrates that charge transport properties of non-covalent types of single molecule junctions may be tuned by the alteration of the dielectric constant of the environment.

3. Conclusions

We demonstrated that three organic helquat dications without any anchoring group in their structure interact with gold surfaces, enabling thus measurements of single molecule conductance values in the break junction arrangement. Their conductance is strongly affected by the presence of solvent molecules. In water environment the conductance is almost constant and independent of the number of rings in the helquat structure (conjugated path length), whereas in non-polar mesitylene the conductance is almost two orders of magnitude lower and increases with increasing number of rings in helquat series. These studies were complemented by electrochemical characterization, which confirmed the adsorption of helquat molecules in water. We have shown that an increase of molecular junction conductance in the presence of mesitylene solvent correlates with the ability of helquat molecules to accept electron(s) as shown electrochemically by observing less negative standard redox potential values with increasing number of rings in the structure. Theoretical calculations together with the experiments point to an important role of solvent in the determination of molecular junction conductance values.

Experimental Section

Deionized MilliQ water (maximum total organic carbon of 3 ppb, minimum electric resistivity of 18.2 MΩ·cm, Millipore, France) was used throughout the experimental work. All items utilized in the experiments (glassware for the preparation of solutions, electrochemical cell, PTFE liquid cells for STM-BJ and MCBJ measurements, Kalrez O-rings and gold substrates) were cleaned by boiling in 25% nitric acid (Lach-Ner, Czech Republic). Subsequently, the items were

repeatedly boiled in water and dried at 105 °C in an oven overnight.

Synthesis and characterization of helquat molecules were described previously.[3] Argon gas (99.996 %, Messer), mesitylene (1,3,5-trimethylbenzene, 98 %, Sigma-Aldrich) and ethanol (absolute p.a., 99.8 %, Penta, Czech Republic) were used as received. Tetrabutylammonium hexafluorophosphate ($TBAPF_6$) and acetonitrile were of the best quality available from Sigma Aldrich. Acetonitrile was dried over 4 Å activated molecular sieves and $TBAPF_6$ was re-crystallized and dried under vacuum before experiments.

Electrochemical experiments used instrumentation and conditions described in our previous communications.[3,4] Further details are provided in the Supporting Information, Section 6.

Solutions of helquat compounds for the single molecule conductance measurements were prepared in two steps. First, 2×10^{-3} M solution of the respective compound was prepared in ethanol. Then either water or mesitylene was added to achieve the volume ratio of 1:9, forming the final solution with the compound concentration of 2×10^{-4} M and the ethanol content of 10 %. In both environments, the introduction of ethanol to the investigated system at this concentration level was found to produce no features attributable to single molecule junctions and led to no increase of the instrumental noise level as confirmed by independent control experiments.

The STM BJ technique was employed to investigate charge transport characteristics of single molecule junctions of compounds dissolved in both mesitylene and in the aqueous environment. A gold sheet (10 mm × 10 mm × 1.0 mm, 99.95 %, Goodfellow) served as the STM substrate. The substrate was copiously rinsed with water just before measurements, annealed by a butane flame and cooled down to the room temperature under the stream of argon. A PTFE liquid cell equipped with a Kalrez O-ring was placed on the top of the substrate and the cell assembly was finalized by the introduction of the solution to the cell. STM probes were prepared by electrochemical etching of the gold wire (0.25 mm diameter, 99.99 %, Goodfellow). Etched probes were copiously rinsed with water, dried and used for measurements in mesitylene solvent. For water-based measurements the probes were additionally coated by polyethylene to eliminate parasitic contributions to the electric current from the polar solvent. For both environments the probe approach and retraction rate was set to 360 and 36 nm/s, respectively and bias voltage value was set to 130 mV. All STM BJ measurements were carried out at ambient temperature and pressure.

The MCBJ technique was employed to investigate single molecule charge transport characteristics of compounds dissolved in mesitylene. A gold wire (99.999 %, Goodfellow, 0.1 mm diameter) was suspended on two freshly prepared droplets of insulating epoxy resin (Stycast 2850FT with catalyst 9) cast on a spring steel sheet (30 mm × 10 mm × 0.2 mm). Upon fixing the gold wire, the epoxy resin was cured at 60 °C overnight. Subsequently, the gold wire was notched between the two epoxy droplets by a scalpel blade to define a constriction point for the junction opening. A PTFE liquid cell equipped with a Kalrez O-ring was placed on the top of such a device and the solution was introduced to the cell. Two electrodes were created by breaking the gold wire at the constriction point by a stepper motor positioned below the spring steel sheet. Bias voltage was set to 130 mV. All MCBJ measurements were carried out at ambient temperature and pressure. Further details on the STM BJ and MCBJ technique can be found in Šebera et al.[27]

Computational Methods

In order to describe the charge transport through helquat molecules we performed calculations based on Density Functional Theory (DFT) and non-equilibrium Green's function (NEGF) formalism.[32–34] Our computational model includes two Au_{18} ($2\times3\times3$) clusters representing left and right electrode and [5]helquat or [6]helquat and [7]helquat molecules with two $CF_3SO_3^-$ counterions and 15 water molecules. This model was geometry-optimized by DFT PBE functional[35,36] using D3 dispersion coefficient[37] and def-SV(P) basis set[38–40] for all atoms, for core 60 electrons of Au the relativistic pseudopotential (effective core potential) def-ecp was used.[41] The Au bond length in Au_{18} clusters was fixed to 2.885 Å (experimental value of bulk gold bond)[42] and the mutual position of the clusters was fixed based on the experimental distance of electrodes as determined from STMBJ 2D conductance-distance histograms. For all gradient optimization tasks the computational chemistry program Turbomole-7.1 was used.[43,44] To investigate the possible geometry configurations of helquat molecules between Au_{18} clusters, we performed gradient optimization procedure from four initial geometries where molecule was rotated by 90° in the plane which was coplanar to the planes of surfaces of Au_{18} clusters. In the second step, the transmission function $\tau(\varepsilon)$ was calculated using the Au_{18}-molecule-Au_{18} computational model based directly on the gradient optimized geometry. Based on four geometry-optimized configurations only that configuration with the lowest energy was taken as the representative one (highlighted in Table S-1 of the SI). This configuration was also used for calculation of transmission functions in the absence of water molecules (here referred to as vacuum).

The transmission function curves $\tau(\varepsilon)$ were calculated using the Amsterdam density functional (ADF)[45,46] version 2017[47] quantum chemistry package with OPBE[48] DFT functional. A Slater-type double-ξ (DZ)[49] basis set with frozen core approximation FC (the core is defined up to 4f shells) was used for gold atoms, and the Slater-type triple-ξ polarized (TZP)[49] basis set with frozen core approximation (the core is defined up to 3p shells for S, 2 s shells for F,C,N,O) was used for the atoms included in the investigated molecules except for hydrogen atom where all electrons TZP basis set was used. Theoretical calculations in ADF program were done with the incorporation of relativistic effects at the level of zero-order regular approximation (ZORA) in a scalar relativistic form of Dirac relativistic equation.[49–51] Theoretical conductance was calculated based on Landauer formula $G = G_0\tau(\varepsilon_F)$ using zero bias voltage approximation, where $\tau(\varepsilon_F)$ represents the transmission function at the Fermi energy ε_F of the gold electrodes. The Fermi energy $\varepsilon_F = -5.1\pm0.1$ eV was estimated on the basis of the experimentally-obtained work function for polycrystalline gold.[52,53] Theoretical conductance G^{th} was based on an average of all calculated G values taken from the transmission function in the interval from −5.0 eV to −5.2 eV. The first redox potentials E_1^0 and energies of HOMO/LUMO orbitals of all investigated molecules were calculated using DFT functional B3LYP[54,55] using cc-pVTZ[56] basis set. The acetonitrile solvent was described by Polarizable Continuum Model (PCM)[57] as implemented in quantum chemistry program Gaussian 09.[58] Further details are given elsewhere.[16]

Acknowledgements

This research was supported by the Czech Science Foundation GAČR (project 18-04682S) and by the Czech Academy of Sciences (RVO 61388963, RVO 61389955).

Keywords: helquats · single molecule conductance · break junction methods · electrochemistry · solvent effect

[1] K. Dhbaibi, L. Favereau, J. Crassous, *Chem. Rev.* **2019**, *119*, 8846–8953.
[2] M. S. Newman, W. B. Lutz, D. Lednicer, *J. Am. Chem. Soc.* **1955**, *77*, 3420–3421.
[3] L. Adriaenssens, L. Severa, T. Šálová, I. Císařová, R. Pohl, D. Šaman, S. V. Rocha, N. S. Finney, L. Pospíšil, P. Slavíček, T. Teplý, *Chem. Eur. J.* **2009**, *15*, 1072–1076.
[4] L. Pospíšil, F. Teplý, M. Gál, L. Adriaenssens, M. Horáček, L. Severa, *Phys. Chem. Chem. Phys.* **2010**, *12*, 1550–1556.
[5] L. Pospíšil, L. Bednárová, P. Štěpánek, P. Slavíček, J. Vávra, M. Hromadová, H. Dlouhá, J. Tarábek, F. Teplý, *J. Am. Chem. Soc.* **2014**, *136*, 10826–1082.
[6] I. Rončević, L. Severa, P. E. Reyes-Gutierrez, L. Bednárová, M. Hromadová, L. Pospíšil, *ChemElectroChem* **2019**, *6*, 3002–3008.
[7] Z. Krausová, P. Sehnal, B. P. Bondzic, S. Chercheja, P. Eilbracht, I. G. Stará, D. Šaman, I. Starý, *Eur. J. Org. Chem.* **2011**, 3849–3857.
[8] M. A. Shcherbina, X. Zeng, T. Tadjiev, G. Ungar, S. H. Eichhorn, K. E. S. Phillips, T. J. Katz, *Angew. Chem. Int. Ed.* **2009**, *48*, 7837–7840; *Angew. Chem.* **2009**, *121*, 7977–7980.
[9] J. Vacek, J. Hrbáč, T. Strašák, V. Církva, J. Sýkora, L. Fekete, J. Pokorný, J. Bulíř, M. Hromadová, J. Crassous, J. Storch, *ChemElectroChem* **2018**, *5*, 2080–2088.
[10] P. Rahe, M. Nimmrich, A. Greuling, J. Schütte, I. G. Stará, J. Rybáček, G. Huerta-Angeles, I. Starý, M. Rohlfing, A. Kühnle, *J. Phys. Chem. C* **2010**, *114*, 1547–1552.
[11] L. E. R. Buckley, B. J. Coe, D. Rusanova, S. Sánchez, M. Jirásek, V. D. Joshi, J. Vávra, D. Khobragade, L. Pospíšil, Š. Ramešová, I. Císařová, D. Šaman, R. Pohl, K. Clays, N. Van Steerteghem, B. S. Brunschwig, F. Teplý, *Dalton Trans.* **2017**, *46*, 1052–1064.
[12] H. Isla, J. Crassous, *C. R. Chim.* **2016**, *19*, 39–49.
[13] J. R. Brandt, L. Pospíšil, L. Bednárová, R. Correa da Costa, A. J. P. White, T. Mori, F. Teplý, M. J. Fuchter, *Chem. Commun.* **2017**, *53*, 9059–9062.
[14] J. R. Quinn, F. W. Foss Jr., L. Venkataraman, R. Breslow, *J. Am. Chem. Soc.* **2007**, *129*, 12376–12377.
[15] V. Kolivoška, M. Valášek, M. Gál, R. Sokolová, J. Bulíčková, L. Pospíšil, G. Mészáros, M. Hromadová, *J. Phys. Chem. Lett.* **2013**, *4*, 589–595.
[16] Š. Nováková Lachmanová, J. Šebera, V. Kolivoška, J. Gasior, G. Mészáros, G. Dupeyre, P. P. Lainé, M. Hromadová, *Electrochim. Acta* **2018**, *264*, 301–311.
[17] J. Šebera, T. Sebechlebská, Š. Nováková Lachmanová, J. Gasior, P. Moreno Garcia, G. Mészáros, M. Valášek, V. Kolivoška, M. Hromadová, *Electrochim. Acta* **2019**, *301*, 267–273.
[18] I. Bâldea, *Nanoscale* **2013**, *5*, 9222–9230.
[19] V. Fatemi, M. Kamenetska, J. B. Neaton, L. Venkataraman, *Nano Lett.* **2011**, *11*, 1988–1992.
[20] D. C. Milan, O. A. Al-Owaedi, M.-Ch. Oerthel, S. Marqués-González, R. J. Brooke, M. R. Bryce, P. Cea, J. Ferrer, S. J. Higgins, C. J. Lambert, P. J. Low, D. Z. Manrique, S. Martin, R. J. Nichols, W. Schwarzacher, V. M. García-Suárez, *J. Phys. Chem. C* **2016**, *120*, 15666–15674.
[21] L. L. Peng, F. Chen, Z. W. Hong, J. F. Zheng, L. Fillaud, Y. Yuan, M. L. Huang, Y. Shao, X. S. Zhou, J. Z. Chen, E. Maisonhaute, *Nanoscalee* **2018**, *10*, 7026–7032.
[22] N. Clément, D. Guérin, S. Pleutin, S. Godey, D. Vuillaume, *J. Phys. Chem. C* **2012**, *116*, 17753–17763.
[23] R. de Levie, L. Pospíšil, *J. Electroanal. Chem.* **1969**, *22*, 277–290.
[24] L. Pospíšil, *J. Electroanal. Chem.* **1976**, *74*, 369–376.
[25] P. Delahay, *J. Phys. Chem.* **1966**, *70*, 2373–2379.
[26] M. Hromadová, V. Kolivoška in *Encyclopedia of Interfacial Chemistry: Surface Science and Electrochemistry, Vol. 5* (Ed. K. Wandelt), Elsevier **2018**, pp. 271–280.
[27] J. Šebera, V. Kolivoška, M. Valášek, J. Gasior, R. Sokolová, G. Mészáros, W. Hong, M. Mayor, M. Hromadová, *J. Phys. Chem. C* **2017**, *121*, 12885–12894.
[28] J. M. Heras, L. Viscido, *Appl. Surf. Sci.* **1980**, *4*, 238–241.
[29] D. C. Milan, O. A. Al-Owaedi, M. C. Oerthel, S. Marqués-González, R. J. Brooke, M. R. Bryce, P. Cea, J. Ferrer, S. J. Higgins, C. J. Lambert, P. J. Low, D. Z. Manrique, S. Martin, R. J. Nichols, W. Schwarzacher, V. M. García-Suárez, *J. Phys. Chem. C* **2016**, *120*, 15666–15674.
[30] J. Nejedlý, M. Šámal, J. Rybáček, M. Tobrmanová, F. Szydlo, Ch. Coudret, M. Neumeier, J. Vacek, J. Vacek Chocholoušová, M. Budešínský, D. Šaman, L. Bednárová, L. Sieger, I. G. Stará, I. Starý, *Angew. Chem. Int. Ed.* **2017**, *56*, 5839–5843; *Angew. Chem.* **2017**, *129*, 5933–5937.
[31] J. Vacek, J. Vacek Chocholoušová, I. G. Stará, I. Starý, Y. Dubi, *Nanoscale* **2015**, *7*, 8793–8802.
[32] M. Brandbyge, J. L. Mozos, P. Ordejón, J. Taylor, K. Stokbro, *Phys. Rev. B* **2002**, *65*, 165401 (pp 17).
[33] J. M. Soler, E. Artacho, J. D. Gale, A. García, J. Junquera, P. Ordejón, D. Sánchez-Portal, *J. Phys. Condens. Matter* **2002**, *14*, 2745–2780.
[34] K. Stokbro, D. E. Petersen, S. Smidstrup, A. Blom, M. Ipsen, K. Kaasbjerg, *Phys. Rev. B* **2010**, *82*, 075420 (pp. 7).
[35] J. P. Perdew, Y. Wang, *Phys. Rev. B* **1992**, *45*, 13244–13249.
[36] J. P. Perdew, K. Burke, M. Ernzerhof, *Phys. Rev. Lett.* **1996**, *77*, 3865–3868.
[37] S. Grimme, J. Antony, S. Ehrlich, H. Krieg, *J. Chem. Phys.* **2010**, *132*, 154104 (pp 19).
[38] A. Schäfer, H. Horn, R. Ahlrichs, **1992**, *97*, 2571–2577.
[39] K. Eichkorn, O. Treutler, H. Ohm, M. Haser, R. Ahlrichs, *Chem. Phys. Lett.* **1995**, *242*, 652–660.
[40] K. Eichkorn, F. Weigend, O. Treutler, R. Ahlrichs, *Theor. Chem. Acc.* **1997**, *97*, 119–124.
[41] D. Andrae, U. Häußermann, M. Dolg, H. Stoll, H. Preuß, *Theor. Chim. Acta* **1990**, *77*, 123–141.
[42] *Handbook of Nanoscopy*, *Vol. 2* (Eds. G. Van Tendeloo, D. Van Dyck, S. J. Pennycook), John Wiley & Sons, **2012**.
[43] R. Ahlrichs, M. Bär, M. Häser, H. Horn, C. Kölmel, *Chem. Phys. Lett.* **1989**, *162*, 165–169.
[44] F. Furche, R. Ahlrichs, C. Hattig, W. Klopper, M. Sierka, F. Weigend, *WIREs Comput. Mol. Sci.* **2014**, *4*, 91–100.
[45] G. te Velde, F. M. Bickelhaupt, E. J. Baerends, C. Fonseca Guerra, S. J. A. van Gisbergen, J. G. Snijders, T. Ziegler, *J. Comput. Chem.* **2001**, *22*, 931–967.
[46] C. Fonseca Guerra, J. G. Snijders, G. te Velde, E. J. Baerends, *Theor. Chem. Acc.* **1998**, *99*, 391–403.
[47] ADF2017, SCM, Theoretical Chemistry, Vrije Universiteit, Amsterdam, The Netherlands, http://www.scm.com
[48] M. Swart, A. W. Ehlers, K. Lammertsma, *Mol. Phys.* **2004**, *102*, 2467–2474.
[49] E. van Lenthe, E. J. Baerends, *J. Comput. Chem.* **2003**, *24*, 1142–1156.
[50] E. van Lenthe, E. J. Baerends, J. G. Snijders, *J. Chem. Phys.* **1994**, *101*, 9783–9792.
[51] E. van Lenthe, A. Ehlers, E. J. Baerends, *J. Chem. Phys.* **1999**, *110*, 8943–8953.
[52] S. C. Veenstra, U. Stalmach, V. V. Krasnikov, G. Hadziioannou, H. T. Jonkman, A. Heeres, G. A. Sawatzky, *Appl. Phys. Lett.* **2000**, *76*, 2253–2255.
[53] M. L. Trouwborst, E. H. Huisman, F. L. Bakker, S. J. van der Molen, B. J. van Wees, *Phys. Rev. Lett.* **2008**, *100*, 175502 (pp. 4).
[54] A. D. Becke, *J. Chem. Phys.* **1993**, *98*, 5648–5652.
[55] C. T. Lee, W. T. Yang, R. G. Parr, *Phys. Rev. B* **1988**, *37*, 785–789.
[56] T. H. Dunning Jr., *J. Chem. Phys.* **1989**, *90*, 1007–1023.
[57] J. Tomasi, B. Mennucci, R. Cammi, *Chem. Rev.* **2005**, *105*, 2999–3094.
[58] *Gaussian 09, Revision E.01*, M. J. Frisch, G. W. Trucks, H. B. Schlegel, G. E. Scuseria, M. A. Robb, J. R. Cheeseman, G. Scalmani, V. Barone, G. A. Petersson, H. Nakatsuji, X. Li, M. Caricato, A. Marenich, J. Bloino, B. G. Janesko, R. Gomperts, B. Mennucci, H. P. Hratchian, J. V. Ortiz, A. F. Izmaylov, J. L. Sonnenberg, D. Williams-Young, F. Ding, F. Lipparini, F. Egidi, J. Goings, B. Peng, A. Petrone, T. Henderson, D. Ranasinghe, V. G. Zakrzewski, J. Gao, N. Rega, G. Zheng, W. Liang, M. Hada, M. Ehara, K. Toyota, R. Fukuda, J. Hasegawa, M. Ishida, T. Nakajima, Y. Honda, O. Kitao, H. Nakai, T. Vreven, K. Throssell, J. A. Montgomery, Jr., J. E. Peralta, F. Ogliaro, M. Bearpark, J. J. Heyd, E. Brothers, K. N. Kudin, V. N. Staroverov, T. Keith, R. Kobayashi, J. Normand, K. Raghavachari, A. Rendell, J. C. Burant, S. S. Iyengar, J. Tomasi, M. Cossi, J. M. Millam, M. Klene, C. Adamo, R. Cammi, J. W. Ochterski, R. L. Martin, K. Morokuma, O. Farkas, J. B. Foresman, D. J. Fox, Gaussian, Inc., Wallingford CT, **2016**.

Manuscript received: October 24, 2019
Revised manuscript received: November 19, 2019
Accepted manuscript online: November 20, 2019